Molecular Simulations of Dense Hydrothermal NaCl−H_2O Solutions from Subcritical to Supercritical Conditions

Matthew T. Reagan, Jonathan G. Harris, and Jefferson W. Tester*,†

Department of Chemical Engineering and Energy Laboratory, Massachusetts Institute of Technology, Room E40-455, Cambridge, Massachusetts 02139-4307

Received: March 3, 1999; In Final Form: June 18, 1999

This research has demonstrated that simple structural and potential models can qualitatively and quantitatively predict properties in dense hydrothermal solutions of sodium chloride and water using molecular dynamics simulation. The $PT\rho x_i$ behavior of simulated model systems at 250 bar and 21 wt % NaCl compared favorably to experimental data from ambient to near-critical temperatures as represented by the Anderko−Pitzer equation of state. The system internal energy, including both dispersion and electrostatic contributions, was computed for a range of temperatures from 177 to 727 °C at 250 bar and found to be realistic in terms of the known thermodynamic properties of water. Radial distribution functions indicate little change in water structure from ambient to near-critical temperatures but large changes in ion association consistent with experimental observation. We found that varying system pressure from 250 to 1000 bar does not noticeably affect solution structure or ion association at subcritical conditions.

Introduction

Aqueous NaCl solutions are found in chemical, industrial, geochemical, and biological processes, and as such have been actively studied for over a century. However, recent developments in supercritical water oxidation (SCWO) have created new interest in the physical properties of these solutions at high temperatures and pressures where far less data are available for engineering applications.[1]

Several experimental studies have examined the solubility of sodium chloride, a common byproduct of SCWO processes, and other studies have determined the phase behavior of sodium chloride−water solutions near the solution critical point.[2−10] Typically, data requirements for SCWO exceed what are available from extensive hydrochemical studies, particularly in the temperature range from 300 to 650 °C over pressures from 200 to 400 bar.[5,11−13] In addition to experimental measurements, advances in computing power have made molecular simulation a viable technique for studying the structure and properties of hydrothermal, near-critical, and supercritical salt solutions.

Previous simulation studies have examined the behavior of pure water and water−salt systems at ambient and supercritical conditions. The bulk of these studies have looked at supercritical ion solvation at infinite dilution and calculated potentials of mean force for isolated ion pairs. Smith and Dang examined Na−Cl ion pairs in both polarizable and rigid water simulation and compared dilute solutions to bulk water properties.[14] Chialvo and co-workers expanded the study of Na−Cl ion pairs to examine the effect of intermolecular potential models and to calculate the association constant and compare it to electrical conductance measurements.[15] Harris and Cui used molecular dynamics (MD) and the rigid SPC model to estimate the solubility and activity coefficients of NaCl in supercritical water and calculate the potential of mean force for the Na−Cl ion pair.[16] Expanding the investigation to finite concentrations, Cummings and co-workers examined the structure of SPC water solutions at supercritical conditions and established a baseline of qualitative results for supercritical solution structure.[17] Hummer and collaborators examined a 21 wt % dense NaCl brine at a single temperature and fixed density [18] as part of a comparison of RISM, Monte Carlo (MC), and MD methods in the development of a new reaction-field formulation.[19] A similar, more concentrated system at 28 wt % was simulated by Rode,[20] from gaseous to liquid densities at subcritical temperatures, giving a first look at ion association in low-density systems and the overall effect on solution structure. More recently, Driesner and collaborators have also studied ion association and hydration structure at concentrations of 1 molal NaCl and temperatures up to 317 °C. [21] In another recent study, Brodholt has used the SPC/E model to simulate NaCl solutions from infinite dilution to 23 wt % at pressures up to 5000 bar.[22] These studies give new insight into the behavior of high-temperature brines at high densities. However, no molecular simulation study has comprehensively examined simple potential models under the conditions encountered during the treatment of chlorinated wastes in practical SCWO processes.[1,5,11−13] Therefore, in this study we aim to examine the behavior of such dense brines from near-ambient to supercritical temperatures at a pressure of 250 bar.

In this study, the usefulness of simple models to simulate complex macroscopic behavior of concentrated solutions was evaluated at hydrothermal conditions. In particular, we utilized the popular simple point charge (SPC) model for water and examined the physical properties, solution structure, and ion association in dense brines from near-ambient to supercritical conditions. Our goal was not to gather detailed statistics regarding the behavior and performance of a particular intermolecular potential model in comparison to others, but rather to explore the use of molecular modeling in an engineering context.

Potential Models and Computational Methods

In this study, the interactions between water molecules and ionic species were modeled with the potential model introduced

† Tel: (617) 253-3401. Fax: (617) 253-8013. E-mail: testerel@mit.edu.

10.1021/jp990757g CCC: $18.00
Published on Web 08/31/1999

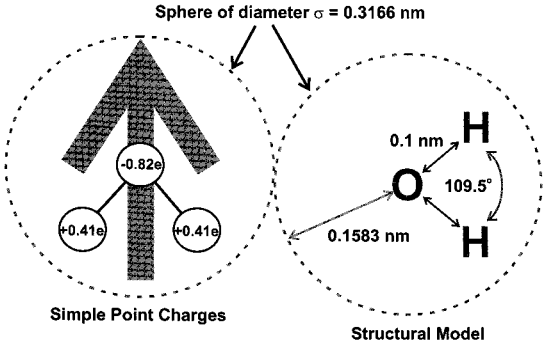

Figure 1. Simple point charge (SPC) model for water.[25]

by Pettit and Rossky.[23] Work by Strauch and Cummings[24] has demonstrated the utility of this model for representing the dielectric properties of water. Pettit and Rossky used the rigid SPC model for water introduced by Berendsen[25] (Figure 1) which includes a Lennard-Jones potential, centered on the oxygen site, with a well depth ϵ of 0.648 kJ/mol and a core diameter σ of 0.3166 nm between oxygen centers. Point charges of -0.82e at the oxygen center and $+0.41$e at each hydrogen site interact through an additional Coulomb potential and represent the permanent dipole moment of water of 2.22 D. Thus,

$$\Phi(r)_{\text{water-water}} = \Phi(r)^{\text{O-O}}_{\text{Lennard-Jones}} + \sum_{\text{site-site}} \Phi(r)_{\text{Coulombic}} \quad (1)$$

where

$$\Phi(r)_{\text{Lennard-Jones}} = 4\epsilon_{ij}\left[\left(\frac{\sigma_{ij}}{r}\right)^{12} - \left(\frac{\sigma_{ij}}{r}\right)^{6}\right] \quad (2)$$

$$\Phi(r)_{\text{Coulombic}} = \frac{1}{4\pi\epsilon_0}\frac{q_i q_j}{r} \quad (3)$$

where ϵ_0 is the vacuum permittivity (e^2 kJ^{-1} mol nm^{-1}), σ_{ij} the soft sphere diameter (nm), ϵ_{ij} the potential well depth (kJ/mol), and r the site−site interatomic separation (nm).

The ions also interact electrostatically through a Coulomb potential (eq 3), and a dispersion interaction captured with a Huggins−Mayer potential[26] that uses specific parameters for sodium and chloride ions regressed from data derived from the work of Fumi and Tosi.[27,28] Equations for the ion−ion interactions are given as

$$\Phi(r)_{\text{ion-ion}} = \Phi(r)_{\text{Huggins-Mayer}} + \sum_{\text{site-site}} \Phi(r)_{\text{Coulombic}} \quad (5)$$

$$\Phi(r)_{\text{Huggins-Mayer}} = B_{ij}\exp(-r/\rho^0_{ij}) - \frac{C_{ij}}{r^6} \quad (6)$$

where C_{ij} is the attractive dispersion parameter (kJ/mol) and B_{ij} and ρ^0_{ij} are the soft core repulsion parameters (kJ/mol, nm).

The water−ion interactions use a Lennard-Jones potential with independent ion−water parameters and a Coulombic interaction between the SPC charges in water and the ion charges.[23] Thus

$$\Phi(r)_{\text{water-ion}} = \Phi(r)^{\text{O-ion}}_{\text{Lennard-Jones}} + \sum_{\text{site-site}} \Phi(r)_{\text{Coulombic}} \quad (7)$$

A complete set of potential parameters is listed in Table 1. Site−site interactions were neglected beyond a cutoff radius, R_c, of 0.95 nm ($2.5\sigma_{ij}$) to avoid double-counting interactions

TABLE 1: SPC Water−NaCl Model Parameters

Water−Water Potential				
atom	σ (nm)	ϵ (kJ/mol)	R_c	q (e)
O	0.3166	0.648	2.5σ	−0.82
H	0.1000	0.000	2.5σ	+0.41

Ion−Water Potentials (Using Geometric Mean Mixing Rule)			
ion (X)	$\sigma_{\text{O-X}}$ (nm)	$\sigma_{\text{H-X}}$ (nm)	$\epsilon_{\text{O-X}} = \epsilon_{\text{H-X}}$ (kJ/mol)
Na^+	0.272	0.131	0.560
Cl^-	0.355	0.214	1.504

Ion−Ion Potentials			
H−M parameter	Na−Na	Na−Cl	Cl−Cl
B_{ij} (kJ/mol)	4.0890×10^4	1.21×10^5	3.36×10^5
ρ_{ij} (nm)	0.0317	0.0317	0.0317
C_{ij} (kJ/mol)	1.012×10^{-4}	6.744×10^{-4}	70.45×10^{-4}

across system periodic boundary conditions.[29] To account for long-range interactions, we used the standard long-range correction to the Lennard-Jones potential and the site−site reaction field of Hummer et al. to correct the Coulombic interaction.[18] The method replaces the site−site Coulomb potential with an effective potential:

$$\Phi(r)_{\text{Coulombic}} = \frac{q_i q_j}{4\pi\epsilon_0}\left(\frac{1}{r} - \frac{3}{2R_c} + \frac{r^2}{2R_c^3}\right) \quad (8)$$

where R_c is the cutoff radius as described above. In addition, each dipole with dipole moment d_s contributes a self-energy of $-{}^1/_2 d_s^2/R_c^3$ to the total potential energy of the system to account for the interaction with the dielectric continuum outside the spherical volume defined by the cutoff radius R_c.

The 21 wt % system of 216 SPC water molecules and 17 Na−Cl ion pairs used by Hummer et al. was a starting point for this study.[18] The equations of motion were integrated with a 3.0 fs (3×10^{-15} s) time step using the Verlet algorithm[29] and the RATTLE technique[30,31] to maintain bond-length constraints and compute the net interactions on each rigid water molecule.[32] Isothermal/isobaric simulations were performed using the Nosé−Andersen approach[33] to maintain system pressure at 250 bar. System equilibration was checked by tracking total potential energy and total system energy, and by dividing the simulation into 5000-cycle blocks to check the evolution of statistics over time. Statistical uncertainties (95% confidence intervals) were calculated based on the total number of independent configurations generated as determined by velocity autocorrelation functions. At least 2500 or more independent configurations were recorded for the calculation of radial distribution functions and structural information. Equilibration runs of 50−150 ps (10^{-12} s) preceded each 250−500 ps production run, corresponding to 50 000 or more sampled configurations.

Simulation Results

Physical Properties. Results of the isobaric/isothermal simulations are given in Table 2. The system was equilibrated at 250 bar, from 177 to 727 °C (450 to 1000 K), with additional data points gathered at 125, 500, and 1000 bar at both 177 °C (450 K) and 327 °C (600 K) for comparison. A fixed-pressure ensemble was used to facilitate comparisons between the simulations and existing experimental data, and to best approximate SCWO process conditions.

TABLE 2: Average Total Dispersion and Electrostatic Energy from MD Simulations (95% Confidence Intervals Indicated in Parentheses)

T (°C)	P (bar)	ρ (g/cm^3)	$\langle\Phi_{disp}\rangle$ (kJ/mol)	$\langle\Phi_{elec}\rangle$ (kJ/mol)
177	250	1.054 (±0.002)	1387.0 (±1.1)	−22795 (±2.0)
227	250	1.008 (±0.002)	1380.7 (±1.5)	−22007 (±1.8)
277	250	0.951 (±0.003)	1340.0 (±1.3)	−21363 (±2.0)
327	250	0.888 (±0.002)	1306.7 (±1.8)	−20751 (±2.3)
377	250	0.764 (±0.005)	1289.4 (±2.7)	−19815 (±5.3)
402	250	0.690 (±0.007)	1276.4 (±2.7)	−19324 (±5.9)
427	250	0.572 (±0.020)	1289.5 (±2.8)	−18645 (±7.7)
452	250	∼0.39[a] (>0.2)	n/a[a]	n/a[a]
452	250	∼0.23[a] (>0.2)	n/a[a]	n/a[a]
477	250	0.188 (±0.001)	1314.2 (±2.9)	−16266 (±5.0)
527	250	0.141 (±0.001)	1304.6 (±2.6)	−15615 (±5.5)
727	250	0.080 (±0.001)	1344.4 (±3.0)	−14216 (±4.6)

[a] Large density fluctuations observed near S−L−V boundary, no single stable equilibrium state.

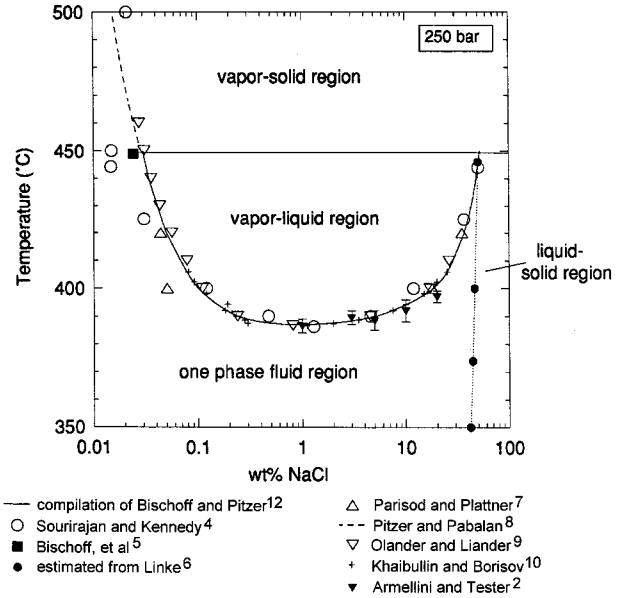

Figure 2. Experimental $T-x_{NaCl}$ diagram for the H_2O−NaCl at 250 bar. Note the log scale for the NaCl composition (adapted from Armellini and Tester[2]).

From the ensemble-average potential energies given in Table 2, we can identify the basic thermodynamic behavior of the model. Below the 402 °C liquid−vapor boundary at 250 bar, the average dispersion energy ($\langle\Phi_{disp}\rangle$, the average total Lennard-Jones/Huggins−Mayer potential energy) decreases with increasing temperature and decreasing density. Above 452 °C, $\langle\Phi_{disp}\rangle$ jumps discontinuously to a higher value. All of these dispersion energies are positive, indicating a net repulsive interaction that becomes less significant as density decreases. The discontinuity around 452 °C represents a fundamental change in the structure of the system—something that would be expected from a phase transition to a single supercritical fluid phase as indicated by experiment (Figure 2). Ensemble-average energies for the 452 °C point could not be estimated due to the inability to equilibrate the system to a stable, single-phase configuration. Generally, the ensemble average electrostatic potential energy, $\langle\Phi_{elec}\rangle$, increases with increasing temperature, representing the transition from solvated ions to insoluble ion pairs. This increasing electrostatic interaction continues from subcritical to supercritical conditions with no discontinuities.

A typical $T-x$ phase diagram for the NaCl−H_2O binary system at 250 bar is given in Figure 2. This phase diagram, taken from the work of Armellini and Tester,[2] combines $T-x$ data from a wide range of experimental studies at 250 bar. Note the inverted vapor−liquid dome present between 393 and 450 °C and the vapor−liquid to vapor−solid transition line that is independent of salt concentration. To assess the volumetric properties of the combined SPC water−NaCl model system over a wider range of $TP\rho x_i$ conditions, the Anderko−Pitzer equation of state[34] (AP-EOS) was used to interpolate existing experimental hydrothermal properties data for the NaCl−H_2O system and to identify phase boundaries. The AP-EOS, developed by Andrej Anderko and Kenneth Pitzer, combines a theoretically based dipolar hard-sphere formulation with an empirical correction based on extensive NaCl−H_2O experimental data. The AP-EOS accurately reproduces the properties of aqueous NaCl solutions under the hydrothermal conditions of interest in this study.[3] A comparison of the AP-EOS generated data to molecular simulation results is shown in Figure 3.

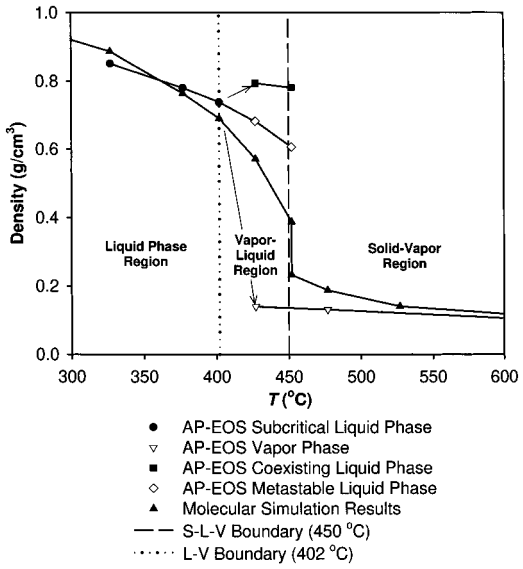

Figure 3. Comparison of experimental and molecular simulation results for the density−temperature behavior of SPC water−21 wt % NaCl at 250 bar. Experimental values generated from the empirically fitted Anderko−Pitzer EOS[34] provided by A. Anderko.[35] Arrows indicate liquid−vapor phase separation in AP-EOS results.

The most notable feature of this comparison is the significant correlation between the density−temperature behavior of the simulated and experimental systems as mapped on the phase diagram. Experimental results at 250 bar (Figure 2) show two transitions along the 21 wt % concentration line: the first a transition to a two-phase liquid−vapor region at 402 °C, and the second a transition to a solid−fluid supercritical region above 450 °C. The AP-EOS also captures these transitions. As seen in Figure 3, the simulated system indicates a rapid drop in total system density across 452 °C, with profound structural instability in simulations performed at this point. Visualizations of the system above and below this point show that the density change is due to a shift from a single-phase bulk system with distributed ions or ion pairs to a nonuniform system of clustered ions suspended in a less dense, nearly pure-water fluid phase. The simulated data point at 452 °C has an unusual degree of uncertainty due to the great difficulty we had equilibrating the system. In fact, these simulations oscillated between two metastable states, one corresponding to ion pairs and small ion clusters with a higher total density (similar to simulation results below $T = 452$ °C) and a lower-density system featuring a single large cluster of ions coexisting with supercritical vapor. Estimated densities for these two metastable states, taken from the instantaneous properties of the system recorded over time,

are included in Table 2. Using the Nosé−Andersen algorithm to maintain constant temperature and pressure, we were not able to converge to a specific stable equilibrium density in this metastable regime.

Quantitatively, the densities reported by the simulation agree well with experimental AP-EOS values at both lower and higher temperatures. Figure 3 compares ensemble-average densities for the SPC water system with three sets of EOS-generated results: liquid-phase density, vapor-phase density, and the density of a hypothetical metastable dense liquid state at the given temperature and pressure.[35] We see some difficulty in modeling the two-phase region from 402 to 450 °C, as the simulation results form a continuous progression from the liquid−vapor region to the solid−vapor region and do not capture direct phase separation behavior. This is expected, since the relatively small 250-molecule system is not large enough to demonstrate true phase separation behavior and the *NPT* constraints mandate a single phase because of Gibbs phase rule considerations. Instead, we see a partial transition to a solid−vapor state as the ion pairs form in solution and begin to form clusters representing nuclei in the formation of a solid phase. This result does not agree with the experimental AP-EOS predictions for a metastable single-phase condition because our simulations contain independent ions, which goes beyond the assumption of fixed ion pairs (molecular NaCl) used by the AP-EOS. In fact, we see a dense liquidlike phase appearing with solid−vapor equilibrium characteristics as temperature increases. To realistically model phase separation in this region, larger multiphase simulations involving 1000−5000 molecules and embedded interfacial structure are currently being studied and the analysis of these systems is planned for a future publication.[36]

Configurational Solution Properties. For each combination of atomic species, we calculated site−site radial distribution functions, g_{O-O}, g_{O-Na}, g_{O-Cl}, g_{Na-Cl}, to capture structural trends in the simulated solutions. Each $g(r)$ was calculated from 2500 independent configurations extracted from the last 250 ps of production. Simulated data were collected into 500 radially oriented bins spaced in equal increments with radius-squared (R^2) scaling for production runs at 250 bar and temperatures ranging from 177 to 727 °C (450 to 1000 K). Figures 4−11 show the complete set of radial distribution functions generated from these simulations.

Figures 4−7 illustrate the subcritical behavior of the system at 250 bar, from 177 to 427 °C. Figure 4 shows little variation in the water structure with temperature below the phase transition point at 450 °C, with no significant change in the position or magnitude of the first or second solvation shells in g_{O-O}. Therefore, despite temperature changes of 250 °C and bulk density changes of 0.5 g/cm^3, a liquidlike structure is maintained throughout the subcritical region.

The water−ion correlation functions, given in Figures 5 and 6, show only a slight decrease in the magnitude of first peak of g_{O-Na} and g_{O-Cl} with increasing temperature, corresponding to a decrease in the average number of water molecules in each ion solvation shell. The calculated g_{O-Cl} also shows a small broadening of the first peak, but no large-scale change in ion solvation behavior between 177 and 402 °C.

In Figure 7, g_{Na-Cl} shows a striking increase in ion−ion association with increasing temperature, which is consistent with a decrease in ion solubility with increasing temperature and decreasing density. This RDF provides semiquantitative confirmation of a gradual transition from fully dissociated, solvated individual ions to ion pairs and ion clusters as we approach

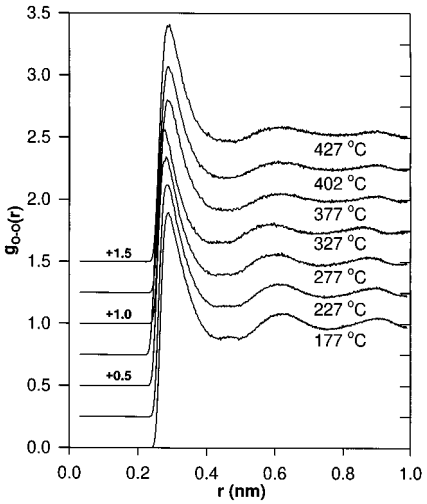

Figure 4. Water−water radial distribution functions for SPC water−21 wt % NaCl MD simulations at 250 bar from 177 to 427 °C. Note: each $g(r)$ is shifted by the indicated amount.

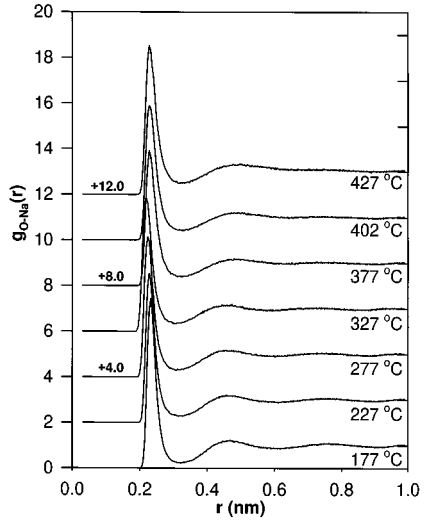

Figure 5. O−Na radial distribution functions for SPC water−21 wt % NaCl MD simulations at 250 bar from 177 to 427 °C. Note: each $g(r)$ is shifted by the indicated amount.

and pass the phase transition point at 450 °C and 250 bar (see Figure 2).

Figures 8−11 illustrate the structural aspects of the supercritical fluid phase of the simulated system. Our calculated correlation functions once again reflect experimental phase behavior in the observed changes to the internal structure of the solution. The water−water correlation function, g_{O-O}, changes dramatically between 427 and 477 °C. Attempts to calculate correlation functions at 452 °C were unsuccessful due to the density fluctuations discussed earlier. Again, we see a shift from a liquidlike structured state to a "combination" state with a correlation function that exhibits features of both liquidlike (solvation shells) and supercritical-like (diffuse clusters) solution structures. This bifurcated condition may be an artifact of the instability of monophase simulations in what should be a two-phase region, since our small system will, at times, display structural properties characteristic of both ordered liquids and vaporlike supercritical fluids. These very different structural effects are intrinsically combined in the orientation- and time-averaged correlation function, resulting in a superposition of two RDF profiles. The $g_{O-O}(r)$ for 727 °C in Figure 8

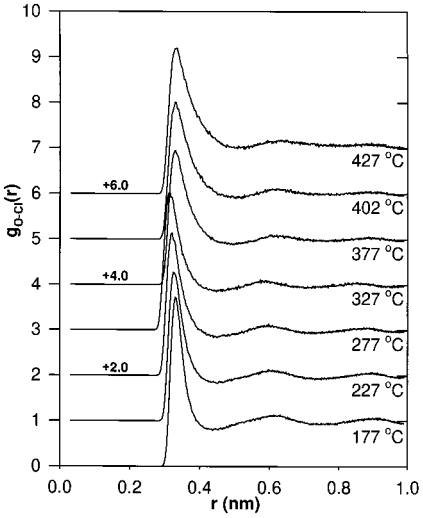

Figure 6. O−Cl radial distribution functions for SPC water−21 wt % NaCl MD simulations at 250 bar from 177 to 427 °C. Note: each $g(r)$ is shifted by the indicated amount.

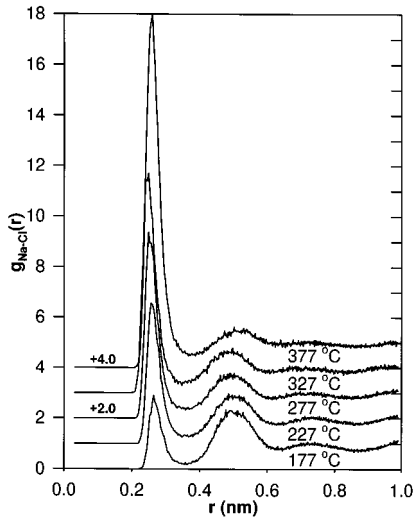

Figure 7. Na-Cl radial distribution functions for SPC water−21 wt % NaCl MD simulations at 250 bar from 177 to 377 °C. Note: each $g(r)$ is shifted by the indicated amount.

contains only a single peak and reflects the structure of a supercritical fluid with local clustering but no long-range structure.

The supercritical-state water−ion correlation functions, $g_{O-Na}(r)$ and $g_{O-Cl}(r)$, are pictured in Figures 9 and 10. Both sets of correlation functions show an overall increase in the magnitude of the first peak up to 527 °C, then a decrease at 727 °C. Once again, we see an increase in the first minimum and second maximum in each RDF, reflecting the combination of two effects: the increased association of ions at higher temperatures and lower densities, plus the continuing hydration of ions at supercritical conditions, noticed by Cui and Harris[16] and other more recent simulation studies.[21] The absolute magnitudes of the 427 °C $g(r)$ plots, when compared with the infinite-dilution molecular NaCl (fixed Na−Cl bond length of 0.23 nm) results of Cui at 427 °C, 246 bar, show a decrease in the first peak by a factor of 3 for both the O−Na and O−Cl RDF. This decrease in ion hydration can be attributed to screening effects caused by high salt concentrations and the possible formation of ion-pair clusters that would disrupt the hydration structure observed in infinite-dilution ion pair studies.[16,15]

Ion association in the supercritical phase is illustrated in Figure 11. In the ion−ion correlation function, g_{Na-Cl}, the magnitude of the first peak increases dramatically above 452 °C, reflecting ion pairs that only associate as pairs or clusters of pairs. If you compare Figure 11 to the subcritical results in Figure 7, you notice that, although the second peak diminishes as we approach 452 °C, once above the phase transition point we see a new, more pronounced second peak, as well as an elevated first minimum. This second peak is shifted outward by 0.1 nm (1 Å) from the subcritical results and increases in magnitude as temperature increases and density decreases. This is consistent with the ordered clustering of ion pairs rather than distributed ions or isolated molecular NaCl. Molecular visualizations of selected steady-state configurations from the simulation confirm these configurational properties. All of these results are consistent with the type of phase transition observed experimentally, and future work intends to characterize the exact structure of these ion clusters near phase transitions.

A concern in RDF analysis of this type is effects of possible density gradients in a relatively small, periodic simulation box. These characteristics have been noted by several authors—an early example in water simulation research includes the simulation studies of the water liquid−vapor interface performed by Townsend and Rice,[37] as well as the NaCl−water research

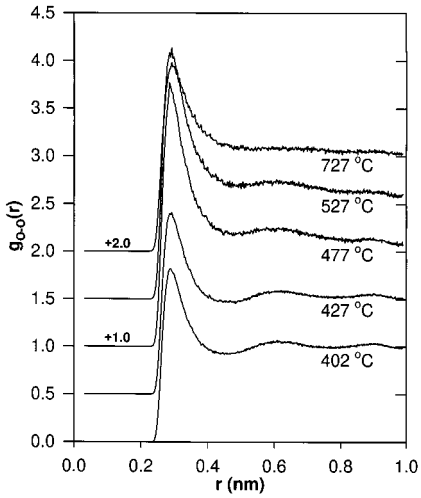

Figure 8. Water−water radial distribution functions for SPC water−21 wt % NaCl MD simulations at 250 bar from 402 to 727 °C. Note: each $g(r)$ is shifted by the indicated amount.

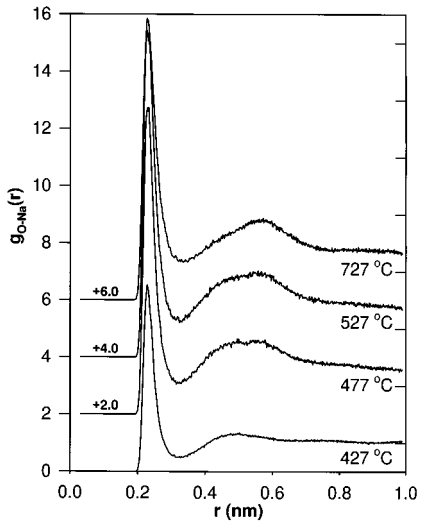

Figure 9. O−Na radial distribution functions for SPC water−21 wt % NaCl MD simulations at 250 bar from 427 to 727 °C. Note: each $g(r)$ is shifted by the indicated amount.

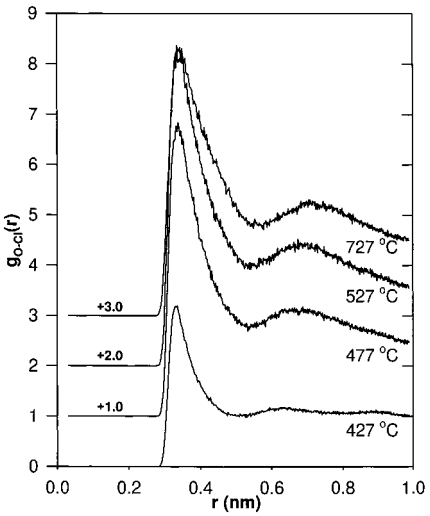

Figure 10. O−Cl radial distribution functions for SPC water−21 wt % NaCl MD simulations at 250 bar from 427 to 727 °C. Note: each $g(r)$ is shifted by the indicated amount.

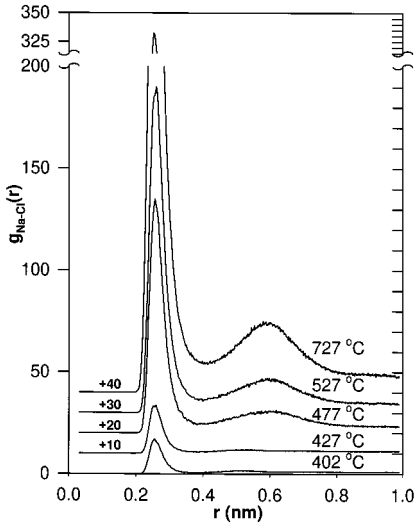

Figure 11. Na−Cl radial distribution functions for SPC water-21 wt % NaCl MD simulations at 250 bar from 402 to 727 °C. Note: each $g(r)$ is shifted by the indicated amount.

published by Rode.[20] In the Townsend study, transverse radial distribution functions taken through regions with a significant density gradient show similar elevated first and second minima. Townsend compares this to a hypothetical, homogeneous "low-density" water generated through *NVT* simulations of ST-2 water. However, we believe that this is better explained by phase separation within a small periodic system. To check this, we calculated the normalized site−site radial density profile, $\rho(r)$, from the 177 and 527 °C water−water radial distribution functions.

$$\rho(r) = (g_{O-O}(r) - 1) \times 4\pi r^2 \qquad (9)$$

At 177 °C, the density profile reaches a maximum near $r =$ 0.31 nm ($r = \sigma_{O-O}$) and then exhibits a consistent oscillation out to $r = 1$ nm and beyond. This demonstrates that in simulated systems approaching liquid density, the assumption that $\rho(r) \rightarrow \langle\rho\rangle$ as r approaches the system periodic boundary clearly holds. However, at 527 °C, the density profile does not decay to zero within the limits of the periodic boundaries. In the simplest terms, there is no large region within the simulation box that has a bulk density equivalent to the average density of the entire simulation system. This reflects clustering or phase

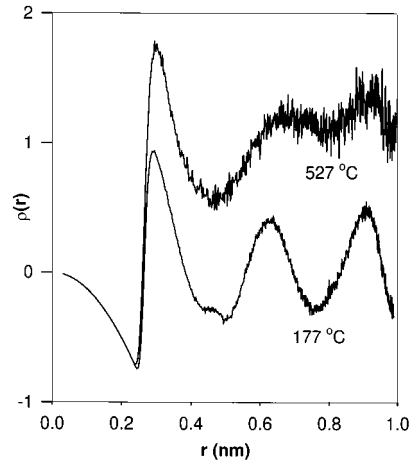

Figure 12. Normalized radial density profiles for SPC water, 21 wt % NaCl MD simulations at 250 bar, subcritical (177 °C), and supercritical (527 °C) temperatures.

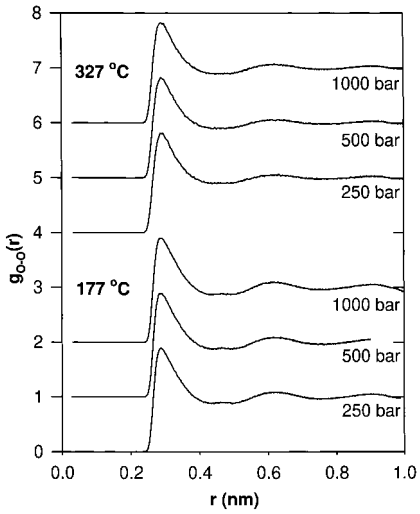

Figure 13. Effect of pressure on water−water radial distribution functions, SPC water, 21 wt % NaCl MD simulations at 250 bar, 177 and 327 °C. Note: each $g(r)$ is shifted upward for clarity.

separation on a length scale approaching the system box size, similar to that shown in the vapor-phase results of Rode,[20] and explains the combination RDFs that contain information suggesting both liquid- and vaporlike phases exist during simulation production.

To gauge the effect of pressure on the solution structure under subcritical conditions, additional simulations were performed at 250, 500, and 1000 bar at 177 and 327 °C. Radial distribution functions, given in Figure 13, indicate that the structure of water does not change noticeably with pressure at these near-ambient density conditions with no shift in the position or magnitude of the first or second peaks in $g(r)$. This trend is expected, as we know that the position of the first peak is largely a function of the potential model rather than of the system density and that with no large density change, the solvation environment will not be greatly affected.

Conclusions

The utility of simple models and potentials for the study of dense sub- and supercritical solutions containing 21 wt % NaCl has been demonstrated. For the quantitative prediction of single-phase densities, we have achieved excellent results using constant-*NPT* molecular dynamics simulations of 216 SPC water molecules and 17 ion pairs, both in replicating the subcritical

regions of the phase diagram and in pinpointing an experimentally determined S−L−V boundary at 450 °C for the NaCl−H_2O system at 250 bar. A key difficulty with this method lies in the restricted variance of the system. The Gibbs phase rule requires a single-phase two-component system to be invariant with three fixed constraints (*NPT*). Due to these restrictions, the two-phase region indicated in the experimental phase diagram and in the Anderko−Pitzer EOS cannot be directly simulated, but only inferred through the system-scale density fluctuations in the simulated system. Our results provide only a total-system bulk density, which represents an average over smaller regions that may exhibit independent liquid- or vaporlike characteristics. The net result is a smooth transition from the single-phase, monovariant $\rho-T$ curve through the two-phase vapor−liquid region. Quantitative predictions for multiphase regions of this system represent a significant area for further study, particularly if you consider that simulations of pure SPC water usually transition to a supercritical phase at temperatures 50−60 °C below the experimental critical point. The fact that our simulated transition from a dense, liquidlike phase to supercritical vapor agrees with experimental measurements, rather than corresponding to a shifted, SPC-specific value, raises new questions about the thermodynamics of aqueous salt systems.

Over the range of $TP\rho x_i$ conditions of interest, calculated radial distribution functions highlight the molecular-level processes that lead to observed macroscopic behavior. First, the anomalous shape of water−water correlation functions through the two-phase region reflects characteristics of both liquid- and vaporlike structure coexisting in our small simulation system. Second, the Na−Cl correlation function clearly shows the mechanics of solvation at work, with individual ions gradually becoming excluded from the solution as temperature increases over a range from 177 to 727 °C. This ion pairing appears despite minimal change in the simulated subcritical water structure below the solution phase transition point at 450 °C. A gradual increase in the total electrostatic potential energy with temperature, independent of density, reflects the thermodynamics of this change from solvated ions to ion pairs.

Additional study of the ion−ion and water−ion RDFs also highlights processes noticed in earlier infinite-dilution work by Cummings and Harris. The change in the shape of the Na−Cl correlation function across the 450 °C transition not only indicates increasing association of ions in pairs, but the formation of a new, elevated second peak and a decrease in overall ion−water correlation reflects the short-range interaction of additional ions, consistent with clusters of two or more bound ion pairs.

Acknowledgment. The authors thank Tomas Arias, Irwin Oppenheim, Gregory Rutledge, Daniel Blankschtein, William Peters, Kenneth Smith, Bernhardt Trout, and Sandeep Patel for lively discussions and input at MIT. Special thanks to Andrej Anderko of OLI Systems for his enormous help in generating the AP-EOS data, and thanks to Peter Cummings and others at Oak Ridge National Laboratory and Athanassis Panagiotopoulos at Cornell for additional insights into this research. This research has been funded through the U.S. Army Research Office and the University Research Initiatives program (DAAL03-92-G-0177-URI), and AASERT grant no. #DAAG04-94-G-0145 under the direction of Robert Shaw.

List of Symbols

T = temperature
P = pressure
$\rho(r)$ = local density
ρ = bulk density
$\Phi(r)$ = interatomic potential energy of interaction
σ = Lennard-Jones soft-sphere diameter
ϵ_{ij} = Lennard-Jones energy well-depth parameter
r = site−site interatomic separation distance
R_c = cutoff radius of interatomic potential
ϵ_0 = vacuum permittivity
q_i = charge on an atom
d_s = dipole moment
B_{ij} = Huggins−Mayer repulsive core parameter
C_{ij} = Huggins−Mayer attractive parameter
ρ_{ij}^0 = Huggins−Mayer repulsive core parameter
$g_{i-j}(r)$ = site−site radial distribution function

References and Notes

(1) Tester, J. W.; Holgate, H. R.; Armellini, F. J.; Webley, P. A.; Killilea, W. R.; Hong, G. T.; Barner, H. E. "Supercritical water oxidation technology: A review of process development and fundamental research"; Emerging Technologies for Hazardous Waste Management, 1993.
(2) Armellini, F. J.; Tester, J. W. *J. Supercrit. Fluids* **1991**, *4*, 254−264.
(3) Tester, J. W.; Marrone, P. A.; DiPippo, M. M.; Sako, K.; Reagan, M. T.; Arias, T. A.; Peters, W. A. *J. Supercrit. Fluids* **1998**, *13*, 225−240.
(4) Sourirajan, S.; Kennedy, G. C. *Am. J. Sci.* **1962**, *260*, 115−141.
(5) Bischoff, J. L.; Rosenbauer, R. J.; Pitzer, K. S. *Geochim. Cosmochim. Acta* **1986**, *50*, 1437.
(6) Linke, W. F. *Solubilities—Inorganic and Metal-Organic Compounds*, 4th ed.; D. Van Nostrand Co. Inc.: New York, 1958.
(7) Parisod, C. J.; Plattner, E. J. *J. Chem. Eng. Data* **1981**, *26*, 1620.
(8) Pitzer, K. S.; Pabalan, R. T. *Geochim. Cosmochim. Acta* **1986**, *50*, 1445−1454.
(9) Olander, A.; Liander, H. *Acta Chim. Scand.* **1950**, *4*, 1437−1445.
(10) Khaibullin, I.; Borisov, N. M. *High Temp.* **1966**, *4*, 489.
(11) Bischoff, J. L.; Pitzer, K. S. *Am. J. Sci.* **1989**, *289*, 217.
(12) Rosenbauer, R. J.; Bischoff, J. L. *Geochim. Cosmochim. Acta* **1987**, *51*, 2349−2354.
(13) Knight, C. L.; Bodnar, R. J. *Geochim. Cosmochim. Acta* **1988**, *53*, 3−8.
(14) Smith, D. E.; Dang, L. X. *J. Chem. Phys.* **1994**, *100*, 3757−3766.
(15) Chialvo, A. A.; Cummings, P. T.; Cochran, H. D.; Simonson, J. M.; Mesmer, R. E. *J. Chem. Phys.* **1995**, *103*, 9379−9387.
(16) Cui, S. T.; Harris, J. G. *Chem. Eng. Sci.* **1994**, *49*, 2749−2763.
(17) Cummings, P. T.; Cochran, H. D.; Simonson, J. M.; Mesmer, R. E.; Karaborni, S. *J. Chem. Phys.* **1991**, *94*, 5606−5621.
(18) Hummer, G.; Soumpasis, D. M.; Neumann, M. *J. Phys. Condens. Matter* **1994**, *6*, A141-A144.
(19) Hummer, G.; Soumpasis, D. M. *Mol. Phys.* **1992**, *77*, 769−785.
(20) Rode, B. M. *Z. Naturforsch.* **1991**, *46a*, 351−356.
(21) Driesner, T.; Seward, T. M.; Tironi, I. G. *Geochim. Cosmochim. Acta* **1998**, *62*, 3095−3107.
(22) Brodholt, J. P. *Chem. Geol.* **1998**, *151*, 11−19.
(23) Pettitt, B. M.; Rossky, P. J. *J. Chem. Phys.* **1986**, *84*, 5836−5844.
(24) Strauch, H. J.; Cummings, P. T. *Mol. Simul.* **1989**, *2*, 89−104.
(25) Berendsen, H. J. C.; Postma, J. P. M.; van Gunsteren, W. F.; Hermans, J. *Jerusalem Symp. Quantum Chem. Biochem.* **1981**.
(26) Huggins, M. L.; Mayer, J. E. *J. Chem. Phys.* **1933**, *1*, 509.
(27) Tosi, M. P.; Fumi, F. G. *J. Phys. Chem. Solids* **1964**, *25*, 45.
(28) Fumi, F. G.; Tosi, M. P. *J. Phys. Chem. Solids* **1964**, *25*, 31.
(29) Allan, M. P.; Tildesley, D. J. *Computer Simulation of Liquids*; Oxford University Press: New York, 1987.
(30) Andersen, H. C. *J. Comput. Phys.* **1983**, *52*, 24−34.
(31) Ryckaert, J. P.; Ciccotti, G.; Berendson, H. J. C. *J. Computat. Phys.* **1977**, *23*, 327−341.
(32) Ciccotti, G.; Ryckaert, J. P. *Comput. Phys. Rep.* **1986**, *4*, 345−392.
(33) Nosé, S. *J. Chem. Phys.* **1984**, *81*, 511−519.
(34) Anderko, A.; Pitzer, K. S. *Geochim. Cosmochim. Acta* **1993**, *57*, 1657−1680.
(35) Anderko, A. Personal communication.
(36) Reagan, M. T.; Tester, J. W. "Molecular modeling of dense sodium chloride−water solutions near the critical point". Presented at the 13th International Conference on the Properties of Water and Steam, Toronto, Ontario, 1999.
(37) Townsend, R. M.; Rice, S. A. *J. Chem. Phys.* **1991**, *94*, 2207−2218.